THE JOURNAL OF PHYSICAL CHEMISTRY LETTERS
A JOURNAL OF THE AMERICAN CHEMICAL SOCIETY

pubs.acs.org/JPCL Letter

Direct Probing of Vibrational Interactions in UiO-66 Polycrystalline Membranes with Femtosecond Two-Dimensional Infrared Spectroscopy

Alexander A. Korotkevich,*[,§] Oleksandr O. Sofronov,[§] Olivier Lugier, Sanghamitra Sengupta, Stefania Tanase, and Huib J. Bakker

Cite This: *J. Phys. Chem. Lett.* 2022, 13, 9793−9800 Read Online

ACCESS | Metrics & More | Article Recommendations | Supporting Information

ABSTRACT: UiO-66 is a benchmark metal−organic framework that holds great promise for the design of new functional materials. In this work, we perform two-dimensional infrared measurements on polycrystalline membranes of UiO-66 grown on c-sapphire substrates. We study the symmetric and antisymmetric stretch vibrations of the carboxylate groups of the terephthalate linker ions and find that these vibrations show a rapid energy exchange and a collective vibrational relaxation with a time constant of 1.3 ps. We also find that the symmetric vibration of the carboxylate group is strongly coupled to a vibration of the aromatic ring of the terephthalate ion. We observe that the antisymmetric carboxylate vibrations of different terephthalate linkers show rapid resonant (Förster) energy transfer with a time constant of ∼1 ps.

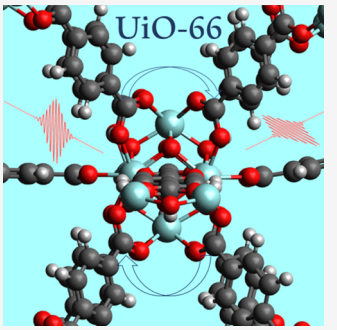

Metal−organic frameworks (MOFs) make up a class of crystalline materials in which metal ions or clusters of metal ions are connected by organic linkers to form extended three-dimensional structures. These materials possess well-defined nanopores and nanochannels, and their size and integrity can be tuned over a wide range by varying the metal cations and linkers.[1−4] As such, different MOF-based functional materials have been prepared and successfully applied in catalysis,[5] chemical sensing,[6] separation techniques,[7] and electrochemistry.[8,9] An important MOF family is UiO, the members of which consist of $Zr_6O_4(OH)_4$ building blocks forming a crystal structure by 12-fold coordination with aromatic dicarboxylate linkers.[10,11] These structures show exceptional stability, even under aggressive conditions, thus making UiOs promising for multiple applications.[12,13] For example, UiO crystalline membranes have been prepared and used for water desalination, gas separation, storage, and pervaporation.[14−16] The range of applications can be further extended by preparing UiO type MOFs for which aromatic dicarboxylate linkers are functionalized.[14,17−19] Such functionalization may thus enable the preparation of stable MOF membranes showing pronounced proton conductivity and/or redox activity, which would be highly promising for designing new fuel cells and electrocatalysis platforms.[18,20]

A crucial parameter determining the properties of UiO membranes is the number density of missing linkers, forming defects in the crystal structure. The deviation from perfect stoichiometry depends on the preparation procedure and often can be controlled, enabling a tuning of the extent of linker−metal interactions.[21−23] The defect content influences the adsorption and separation properties,[24,25] the catalytic activity,[26] and the Brønsted and Lewis acidity[27] of a UiO membrane. The metal−linker interactions are thus very important for the properties of UiO MOFs, and a detailed understanding of these interactions is a prerequisite for the rational design of new UiO-based materials. Various experimental and theoretical approaches have been used to study the dynamics of UiO derivatives. Recent studies addressed the proton conductivity of UiO MOFs,[28] and the role of defects in this process,[29] the dynamics of water adsorbed in the MOF pores,[30] and the relaxation kinetics after excitation of electronic transitions of the linker.[31,32]

A powerful tool for obtaining structural and dynamical information for chemical systems is two-dimensional infrared spectroscopy (2D-IR). By exciting vibrational modes of molecules or ions with femtosecond infrared pulses, this method discloses unique information about the relaxation kinetics of vibrationally excited states, which in turn provides information about vibrational couplings, inter- and intramolecular energy transfer, and the reorientation dynamics of small molecular species. These processes often strongly depend on the solvation and coordination of the target functional

Received: August 12, 2022
Accepted: October 10, 2022

https://doi.org/10.1021/acs.jpclett.2c02509
J. Phys. Chem. Lett. 2022, 13, 9793−9800

groups. Over the past decade, 2D-IR has been successfully applied to investigate the structural elasticity of UiO-66 prepared as powder samples[33] and MIL-53(Al).[34] In this work, we present a 2D-IR investigation of polycrystalline UiO-66 membranes grown on c-sapphire plates. This MOF is the first member of the UiO series and comprises terephthalate (1,4-benzenedicarboxylate, BDC^{2-}) as a linker (Figure 1a).

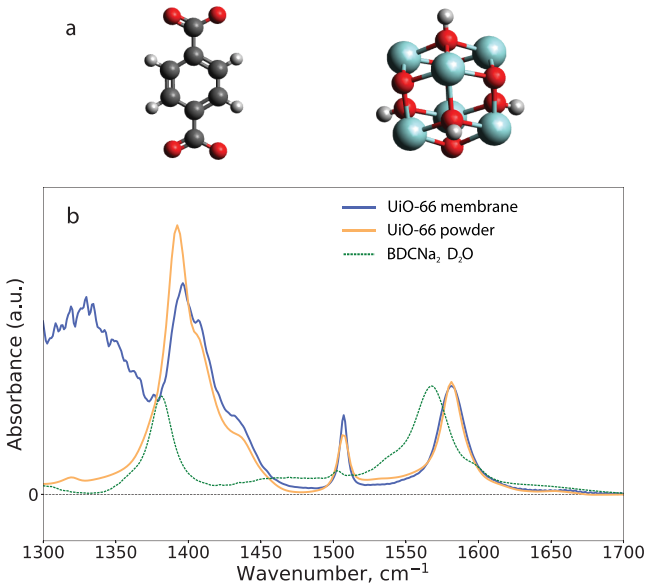

Figure 1. (a) Chemical structures of the terephthalate (BDC^{2-}) linker (left) and $Zr_6O_4(OH)_4$ cluster (right). Black, white, red, and light-blue spheres represent carbon, hydrogen, oxygen, and zirconium atoms, respectively. (b) Linear infrared absorption spectra of UiO-66 membranes grown on a sapphire substrate measured in transmission geometry (blue), UiO-66 powder measured in ATR geometry (orange), and a 0.4 M D_2O solution of disodium terephthalate ($BDCNa_2$, green dashed line). The spectra are normalized with respect to the absorption of the ν_{as} band.

The preparation of UiO-66 membranes on solid substrates is a topic of great current interest. Recently, the preparation of UiO-66 membranes and its derivatives on gold substrates,[14] sapphire rods,[15] α-Al_2O_3 disks,[35] and ZrO_2@γ-Al_2O_3 fibers[36] has been reported. However, to the best of our knowledge, no protocols using flat c-sapphire substrates have been developed. We prepared UiO-66 samples by a solvothermal reaction of $ZrCl_4$ and terephthalic acid ($BDCH_2$) dissolved in dimethylformamide, using acetic acid as a growth modulator. The sample profilometry showed that the membranes are ~600–700 nm thick. The crystallinity of the membranes was confirmed with X-ray diffraction analysis. We find that the grains of the polycrystalline membrane have a preferential (111) orientation and that the membrane preserves the cylindrical symmetry. Thermogravimetric analysis (TGA) shows that this preparation method results in ~42% of missing linkers, which means that the polycrystalline film can be considered a highly defective material. The details of the sample preparation and characterization can be found in the Supporting Information. We further characterize the prepared sample with Fourier transform infrared (FTIR) spectroscopy. In Figure 1b, we compare the infrared absorption spectrum of the prepared UiO-66 membranes with the spectrum of a powder sample. The spectra look very similar in the frequency region above 1400 cm^{-1}, which indicates that the local environment of the linkers is very similar in the film and in the powder. We assign the bands at 1585 and 1395 cm^{-1} to the antisymmetric stretch (ν_{as}) and symmetric stretch (ν_s) vibrations, respectively, of the carboxylate anion groups of the linker. The 1510 cm^{-1} band is assigned to the 19a band of the aromatic ring of the linker (further ν_{Ph}). This ring mode transforms with the same irreducible representation as the ν_s.[37−40] The difference between the spectra at lower frequencies is due to strong sapphire substrate absorption, which precludes a reliable determination of the film absorption values in this frequency region. In our femtosecond 2D-IR experiment, we excite molecular vibrations (ν_s, ν_{Ph}, and ν_{as}) of the terephthalate linker of UiO-66 membranes that absorb in the 6 μm region. We measure the excitation-induced absorption change as a function of the excitation and detection frequencies, the waiting time T between the excitation and detection pulses, and their mutual polarization direction. The isotropic transient absorption dynamics provide information about the dynamics and mechanism of the interactions involving the excited vibrations. The depolarization dynamics of the transient absorption changes reveal the time scale of intermolecular energy transfer between the carboxylate groups of the linkers. An intrinsic challenge related to femtosecond IR experiments on solid samples is the strong scattering of the excitation light by grains of the studied polycrystalline material. This scattering can overwhelm the signal of the weaker infrared detection pulse, and thus, often special techniques such as using index matching liquids[34] or advanced phase cycling schemes[33] have been used to extract reliable data. The UiO-66 membranes that we study scatter light to a much smaller extent than powder samples, and we can sufficiently suppress the remaining scattering by creating a subcycle delay using a wobbler, thus providing another way of overcoming the scattering problem in femtosecond IR studies of MOFs. Sapphire substrates have already been successfully used to grow UiO-66 membranes,[15,16] and their broad transparency window and the absence of significant nonlinear effects upon interaction with intense infrared pulses enable 2D-IR experiments in transmission geometry.

In Figure 2, we show the 2D-IR spectra of the membrane sample. Due to the limited transparency window of sapphire, we can measure the 2D-IR spectra only when $\omega_{detection} > 1500$ cm^{-1}, which excludes a study of the response at $\omega_{detection}$ corresponding to ν_s. However, because the membrane is superposed on the substrate, we are able to detect the transient absorption signals induced by the excitation of ν_s at $\omega_{detection}$ corresponding to ν_{Ph} and ν_{as}.

In Figure 2a, we observe clear responses on the diagonal line at $\omega_{excitation} = \omega_{detection} = 1510$ cm^{-1} and $\omega_{excitation} = \omega_{detection} = 1585$ cm^{-1}, which correspond to the excitation and detection of ν_{Ph} and ν_{as} vibrations, respectively. We also observe several off-diagonal peaks (cross-peaks) indicating a coupling of the different vibrations. In particular, when $\omega_{excitation} = 1395$ cm^{-1} uphill cross-peaks appear at $\omega_{detection} = 1510$ cm^{-1}, indicating vibrational coupling of the ν_s mode to the ν_{Ph} mode ($\nu_s \rightarrow \nu_{Ph}$), and at $\omega_{detection} = 1585$ cm^{-1}, indicating vibrational coupling of the ν_s mode to the ν_{as} mode ($\nu_s \rightarrow \nu_{as}$). When $\omega_{excitation} = 1585$ cm^{-1} and $\omega_{detection} = 1510$ cm^{-1}, we observe a downhill cross-peak indicating vibrational coupling between ν_{as} and ν_{Ph} ($\nu_{as} \rightarrow \nu_{Ph}$).

As one can see in Figure 2b, all signals are still pronounced at a waiting time T of 7 ps, but due to vibrational relaxation,

https://doi.org/10.1021/acs.jpclett.2c02509
J. Phys. Chem. Lett. 2022, 13, 9793−9800

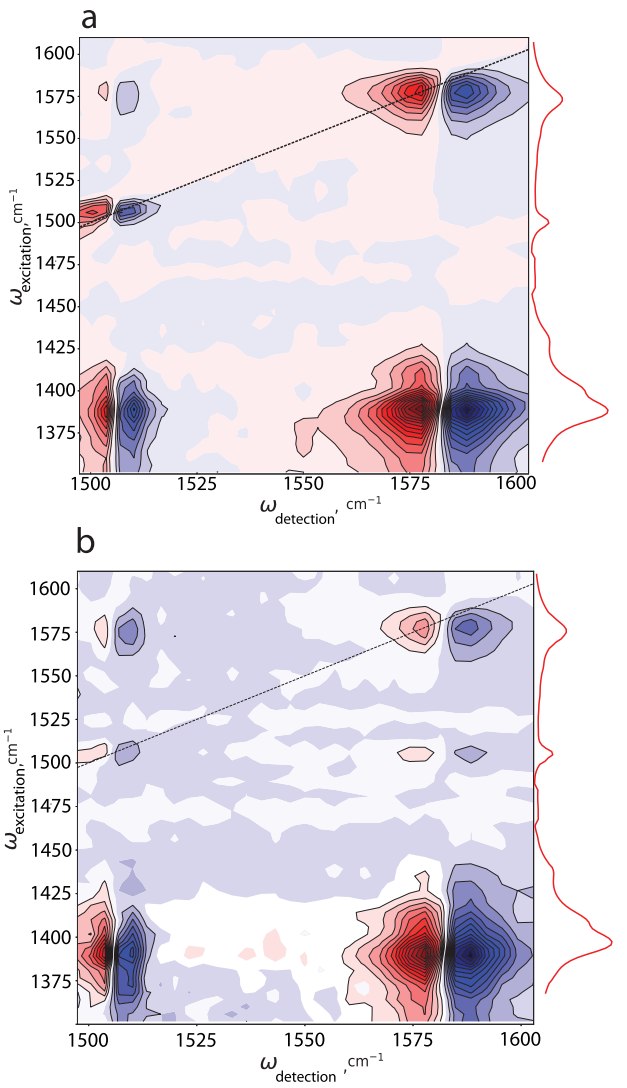

Figure 2. Two-dimensional infrared spectra of UiO-66 membranes grown on sapphire substrates measured at different waiting times. (a) T = 0.3 ps, and (b) T = 7 ps. The spectra are plotted as a function of the excitation frequency (vertical axis) and the detection frequency (horizontal axis). The inset on the right-hand side shows the linear infrared absorption spectrum to clarify the assignment, and the black dashed diagonal line corresponds to $\omega_{detection} = \omega_{excitation}$. The spectra are scaled relative to the transient absorption maxima at each waiting time T.

their relative strengths have become different. The signal of $\nu_{Ph} \rightarrow \nu_{as}$ at $\omega_{excitation}$ = 1510 cm^{-1} and $\omega_{detection}$ = 1585 cm^{-1} becomes more pronounced than at earlier waiting time. Figures 7 and 8 of the Supporting Information show the amplitude of this signal at earlier waiting times.

To identify the mechanism of vibrational relaxation and the nature of the vibrational coupling in UiO-66 membranes, we measure the dynamics of the diagonal and cross-peak signals. In panels a and b of Figure 3, we show the dynamics of the diagonal peak signal corresponding to ν_{as} and the $\nu_s \rightarrow \nu_{as}$ uphill cross-peak. We find that both dynamics can be described well with an exponential relaxation with a time constant of ~1.3 ps to an end level that grows with the same time constant and that shows no further change in amplitude within 200 ps (Figures 8 and 9 of the Supporting Information). The fact that the diagonal ν_{as} and the $\nu_s \rightarrow \nu_{as}$ cross-peak signals show similar relaxation dynamics points to an ultrafast equilibration between the v = 1 states of the ν_{as} and ν_s vibrations, which is most likely due to energy transfer occurring within the time scale of the cross-correlate of the excitation and detection pulses. The growth of the end level can be explained by thermal effects. The energy released as a result of the vibrational relaxation affects the shape and position of the vibrational bands, yielding a change in the transient absorption signal that is often termed a hot-state signal. This signal stays constant on the time scale of the time-resolved experiment because its relaxation relies on heat diffusion out of the excited volume, which typically occurs on a microsecond time scale. Next, we take a closer look at the relaxation dynamics of the transient absorption signals involving the ν_{Ph} vibration. In Figure 3c, we show the dynamics of the diagonal peak corresponding to the excitation and detection of ν_{Ph}. Compared to the dynamics displayed in panels a and b of Figure 3, this signal decays much more slowly, which indicates that the v = 1 state of ν_{Ph} shows a much slower relaxation than the v = 1 states of the stretch vibrations of the carboxylate group. The signal decays to a negligible end level, which means that no pronounced thermal effects are observed for the diagonal signal of the ν_{Ph} vibration. In Figure 3d, we present the dynamics of the $\nu_s \rightarrow \nu_{Ph}$ cross-peak signal. This signal shows a decay that cannot be described well with a single-exponential time constant, and a clear non-zero end level. We find that the dynamics shown in panels c and d of Figure 3 can be consistently described with a model in which the v = 1 state of ν_{Ph} has an intrinsic vibrational relaxation time constant of ~6.7 ps, and in which the ν_{Ph} vibration is coupled to the ν_s vibration by two different mechanisms: anharmonic coupling and energy transfer. The anharmonic coupling leads to an instantaneous perturbation of the vibrational potential of ν_{Ph} following the excitation of the ν_s vibration. This perturbation leads to a frequency shift of the ν_{Ph} vibration, and thus to a transient absorption change at the detection frequency of the ν_{Ph} vibration that will follow the dynamics of the excitation of the ν_s vibration. Therefore, the $\nu_s \rightarrow \nu_{Ph}$ cross-peak signal will show the 1.3 ps decay time constant of the excited ν_s vibration. This component accounts for the fast relaxation component of the cross-peak signal (Figure 3d, blue dashed line). The energy transfer from ν_s to ν_{Ph} leads to a contribution to the cross-peak signal that shows a delayed growth with a time constant ~6.9 ps, followed by a relaxation with a time constant of ~6.7 ps of the vibrational relaxation of the v = 1 state of the ν_{Ph} vibration (Figure 3d, green dashed line). The uphill energy transfer time constant of ~6.9 ps of ν_s to ν_{Ph} is related to a downhill energy transfer time constant of ν_{Ph} to ν_s in accordance with the Boltzmann ratio $k_{up} = k_{down} \exp(-\hbar\Delta\omega/kT)$, where $\Delta\omega$ is the frequency difference between the centers of the absorption bands of ν_s and ν_{Ph}, which is ~100 cm^{-1}. This energy exchange process is accounted for in describing the diagonal ν_{Ph} signal dynamics in Figure 3c. Finally, the growth of the end level of the cross-peak (Figure 3d, red dashed line) is due to the relaxation of the ν_s vibration and the ν_{Ph} vibration, the latter becoming populated as a result of the energy transfer. Given the significantly smaller contribution of the energy transfer to the cross-peak signal, the growth of the end level of the $\nu_s \rightarrow \nu_{Ph}$ cross-peak signal is dominated by the relaxation of the excited ν_s vibration. The signals of the $\nu_{as} \rightarrow \nu_{Ph}$ and $\nu_{Ph} \rightarrow \nu_{as}$ cross-peaks are much weaker than that of the $\nu_s \rightarrow \nu_{Ph}$ cross-peak, as one can see from Figure 2a. By further analyzing the dynamics of these cross-peak signals (see Figure 9 of the

https://doi.org/10.1021/acs.jpclett.2c02509
J. Phys. Chem. Lett. 2022, 13, 9793−9800

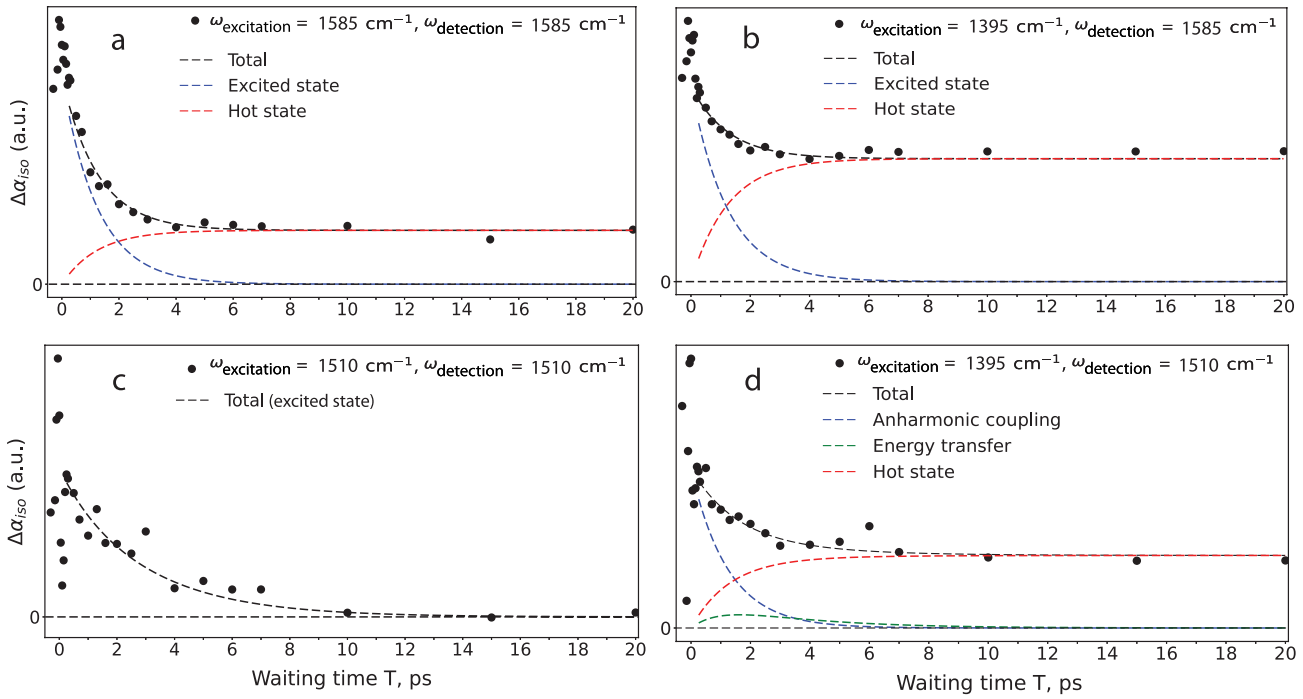

Figure 3. Isotropic transient absorption signals measured for UiO-66 membranes as a function of waiting time T, obtained by integrating the 2D signals over an excitation frequency interval of 20−50 cm^{-1} around the maximum frequency of the absorption bands. (a) Exciting ν_{as} and detecting at the maximum frequency of the ν_{as} band (diagonal ν_{as} signal). (b) Exciting ν_{s} and detecting at the maximum frequency of the ν_{as} band ($\nu_{s} \rightarrow \nu_{as}$ cross-peak signal). (c) Exciting ν_{Ph} and detecting at the maximum frequency of the ν_{Ph} band (diagonal ν_{Ph} signal). (d) Exciting ν_{s} and detecting at the maximum frequency of the ν_{Ph} band ($\nu_{s} \rightarrow \nu_{Ph}$). The black dashed lines represent fits to the dynamics, which contain two or three signal contributions (blue, red, and green dashed lines), according to the model described in the text.

Supporting Information), we conclude that the vibrational coupling between ν_{as} and ν_{Ph} is much weaker than that between ν_{s} and ν_{Ph}. The main coupling mechanism between these vibrations is anharmonic coupling, which implies that the dynamics of the cross-peak signals is determined by that of the excited vibration.

In Figure 4, we show the anisotropy of the excited state of the ν_{as} vibration. To obtain purely the anisotropy dynamics of this excited state, we subtracted the hot-state contributions to the measured $\Delta\alpha_{\parallel}$ and $\Delta\alpha_{\perp}$ signals prior to constructing the anisotropy parameter. The initial anisotropy value is ∼0.4, which is the value expected for isotropic materials. The anisotropy is observed to decay on a picosecond time scale. Considering that in crystalline material the terephthalate linkers are strongly bound to metal ions, reorientation is not expected to take place on a picosecond time scale. Therefore, we conclude that the observed anisotropy decay is due to excitation transfer between closely spaced and differently oriented linker species. Similarly to Nishida et al.,[33] we find that these dynamics can be described well by $Ae^{-\sqrt{(t/\tau)}}$. This expression originates from the Förster model for resonant energy exchange in isotropic materials. We obtain an excitation energy transfer time τ of ∼1 ps.

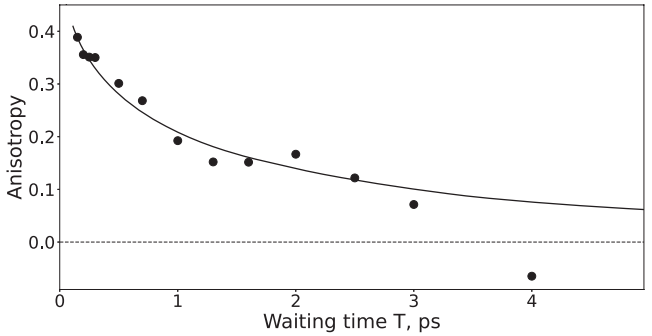

Figure 4. Hot-state corrected anisotropy dynamics of the ν_{as} diagonal peak signal. The solid line represents a fit of the data to a resonant (Förster) energy exchange model.

The infrared absorption spectrum of the terephthalate linker in the UiO-66 structure is quite different from that of the terephthalate dianion in an aqueous solution. First, the cross section of the ν_{s} vibrational mode is almost twice as large as that of the ν_{as} mode in the MOF structure, while in the solution spectrum, these bands have nearly the same amplitude. Interestingly, for disodium terephthalate powder, the cross section of the ν_{s} band is also larger than that of the ν_{as} band, as shown in Figure 4 of the Supporting Information. These findings show that the direct interaction of terephthalate with metal cations leads to a significant redistribution of the charge density and bond strengths in the terephthalate structure, thus significantly altering the transition dipole moments of the carboxylate stretch vibrations. We also find that the absorption band of the ν_{Ph} vibration becomes much stronger in the MOF structure than in terephthalate in aqueous solution. A similar effect is observed for solid disodium terephthalate. The ν_{Ph} vibration has the same symmetry and orientation of its transition dipole as the ν_{s} vibration, and the observed enhancement of the ν_{Ph} vibration is likely due to the interaction between the two vibrations and the increased cross section of the ν_{s} vibration.

We find that the ν_{s} and ν_{as} vibrations of the terephthalate ion show an ultrafast energy equilibration when terephthalate

https://doi.org/10.1021/acs.jpclett.2c02509
J. Phys. Chem. Lett. 2022, 13, 9793−9800

constitutes the linker ion of UiO-66. This result differs from what was observed for the aqueous terephthalate dianion solution. The observations for an aqueous solution indicated the presence of both anharmonic coupling and energy transfer that could be distinguished from each other.[41] This means that most likely the interaction of the terephthalate linker with the Zr^{4+} cations not only changes the cross sections of the ν_s and ν_{as} vibrations but also induces faster energy exchange between these vibrations. The intrinsic vibrational relaxation time constant of ∼1.3 ps that we extract for the equilibrated ν_s and ν_{as} vibrations in the solid sample is very close to the vibrational relaxation time constant of these vibrations observed for aqueous terephthalate, suggesting that the collective vibrational relaxation rate of the carboxylate stretch vibrations is only weakly dependent on the ion environment.

Because of the significant enhancement of the cross section of the ν_{Ph} vibration, we also observe clear transient signals associated with this vibrational mode for UiO-66. We also observe pronounced anharmonic coupling and vibrational energy exchange between ν_{Ph} and ν_s. The interaction between ν_{Ph} and ν_{as} is observed to be much weaker, which can be explained from a simple transition dipole−dipole coupling model.[42] According to this model, the interaction is stronger for ν_{Ph} and ν_s because the transition dipole moments of these vibrational modes are parallel while the transition dipole moments of ν_{as} and ν_{Ph} are perpendicular to each other. The intrinsic vibrational relaxation of the ν_{Ph} mode is observed to be much slower than for the ν_s and ν_{as} vibrations, which indicates that this vibration has a quite different relaxation pathway.

In previous time-resolved vibrational spectroscopy studies of MOFs, the relaxation of other types of vibrations was investigated. For loaded MIL-53(Al) MOFs, the stretching vibration of the deuterated bridging hydroxyl termed μ_2-OD was found to show a relaxation time constant of ∼30−150 ps, depending on the degree of loading.[34] For the C−O stretching vibration of a carbonyl probe-functionalized linker in UiO-66 powder, a bimodal decay was observed, with a 4−5 ps component and a 40−60 ps component.[33] The O−D stretching vibration of μ_2-OD in MIL-53(Al) thus shows a significantly slower relaxation compared to that in aqueous systems.[43−45] At the same time, the vibrations of carboxylate and carbonyl groups of the linker ions in the MOF structure show relaxation rates that are similar to those observed for these vibrations in aqueous or nonpolar solutions.

We observe that the vibrational relaxation of the carboxylate stretch vibrations leads to a significant residual signal associated with the creation of a long-living hot state. The likely reason for this observation is that the linker density is quite high, which implies that a large amount of thermal energy will accumulate in a limited volume following vibrational excitation and relaxation. Such a heating effect is not observed for an aqueous terephthalate solution and is also much less pronounced in a MIL-53(Al) sample, which can be explained well by the much lower density of μ_2-OD groups compared to that of terephthalate linkers in the UiO-66 membranes.

The relative contribution of the hot state to the overall signal is quite different for the diagonal and cross-peak signals shown in Figure 3. For the ν_{as} diagonal peak, we obtain a ratio between the decaying and growing contributions of ∼4, while for the $\nu_s \rightarrow \nu_{as}$ signal, this ratio is ∼1.75. The diagonal signal of ν_{Ph} shows practically no end level, while the cross-peak signal $\nu_s \rightarrow \nu_{Ph}$ shows a clear non-zero end level. The relative amplitude of the hot-state signal depends on the cross sections of the excited and detected vibrations, as well as on the strength of coupling between them. For the cross-peak signal $\nu_s \rightarrow \nu_{Ph}$, the end level is relatively high because the initial signal relies on the anharmonic coupling of the two vibrations, which yields a signal weaker than a diagonal signal, while the final signal (the hot-state end level) is determined by the total energy absorbed from the excitation pulse (see the Supporting Information). The excited ν_s vibration has a large cross section meaning that a large amount of energy is absorbed, thus leading to a relatively strong thermal effect.

The observation of the hot-state signal means that thermalization of the energy of the excited vibrations results in an immediate red-shift of the vibrational bands of the carboxylate group. Recently, similar red-shifts have been shown to indicate a loosening of metal carboxylate linkages in a broad range of carboxylate-based MOFs.[46] Hence, our results show that any heat dissipated in the MOF will lead to a loosening of the MOF linkages on a picosecond time scale. This information is important for further mechanistic studies involving MOFs with a broad range of (photo)catalytic functionalities.

We find that the anisotropy of the excitation of the ν_{as} vibration rapidly decays due to resonant energy transfer between differently oriented terephthalate ions. Interestingly, the ν_{as} vibrations of terephthalate ions in aqueous media show quite slow anisotropy dynamics, which can be explained by the much larger mutual distance of the terephthalate ions in solution. In this case, the anisotropy dynamics primarily result from the reorientation of the ion.[41] It should be noted that the energy transfer between ν_{as} and ν_s does not contribute to the anisotropy decay of ν_{as}, as the accepting mode (ν_s) absorbs at a frequency different from that of the probed mode (ν_{as}). Hence, this energy transfer leads to a change only in the total transient absorption signal at the ν_{as} frequency, but not of the anisotropic character of this signal.

For MIL-53(Al), a limited anisotropy decay for the μ_2-OD vibration was observed, which was explained with a wobbling in a cone model, i.e., orientational diffusion within a limited solid angle.[34] Resonant (Förster) energy transfer has also been observed for the C−O stretching vibration of the carbonyl group that is attached to the aromatic ring of a fraction of terephthalate linkers in UiO-66 powders.[33] In this study, an acceleration of the anisotropy and central line slope dynamics was observed with an increase in the fraction of functionalized linkers.[33] The time scale of the observed decay was significantly longer (10−50 ps), even for the highest functionalized linker loadings (14%), than the ∼1 ps transfer time constant that we find for the anisotropy decay of the ν_{as} vibration of the carboxylate group of the terephthalate linker. This difference can be explained well by the fact that the vibrations of the carboxylate groups of the terephthalate linkers are at a much shorter relative distance than the carbonyl groups of a fraction of functionalized terephthalate linkers. In the UiO-66 structure, the nearest neighbor carboxylate groups are attached to the same Zr^{4+} cation, and thus very close to each other. The rate of transfer between the vibrations of the carboxylate groups is thus expected to be quite sensitive to the linker defect content, which will be the subject of future studies.

In summary, in this work we present a new protocol for the preparation of polycrystalline films of UiO-66 on flat c-sapphire substrates. These MOFs consist of Zr^{4+} ions

https://doi.org/10.1021/acs.jpclett.2c02509
J. Phys. Chem. Lett. 2022, 13, 9793−9800

connected by terephthalate linkers. The advantage of this protocol is that the samples are prepared in a single-step solvothermal process that does not involve preparation of the precursors such as Zr-based clusters. Additionally, to the best of our knowledge, no protocols using flat c-sapphire substrates have been reported. The sapphire substrates have a broad transparency window in the optical frequency range that is promising for applications in photocatalysis and electrochemistry. Furthermore, the membranes prepared according to the protocol contain a high concentration of missing linkers. Highly defective materials have been proven to be applicable in absorptive removal of pollutants,[25] gas separation,[35] and catalysis.[22]

We studied the prepared UiO-66 films with FTIR spectroscopy and 2D-IR spectroscopy in the fingerprint region. Compared to terephthalate ions in aqueous solution, we find that the cross sections of the ν_s carboxylate stretch vibration and ν_{Ph} are strongly enhanced, probably as a result of the interaction with the Zr^{4+} ions. The 2D-IR studies revealed strong vibrational coupling between the ν_s and ν_{as} stretch vibrations of the carboxylate group, as well as between the ν_s vibration and the ν_{Ph} vibrational modes. The ν_{as} and ν_{Ph} modes show a significantly weaker interaction. We find that the ν_s and ν_{as} vibrations show an ultrafast energy exchange and thus relax together with the same effective vibrational relaxation time constant of ~1.3 ps. The absorption of the ν_{Ph} band shows a slower intrinsic vibrational relaxation with a time constant of ~6.7 ps. The ν_s and ν_{Ph} modes are observed to be anharmonically coupled and to show energy exchange, with an uphill energy transfer time constant of ~6.9 ps. The measured transient absorption signals show a significant nonzero signal at long delay times that we attribute to a hot state resulting from vibrational relaxation. We find that the anisotropy dynamics of the excitation of the ν_{as} vibrations can be modeled well with a Förster energy exchange model with a time constant of 1 ps. This relatively fast energy transfer can be explained by the proximity of the carboxylate groups of differently oriented terephthalate linkers in the UiO-66 MOF.

■ ASSOCIATED CONTENT

Supporting Information

The Supporting Information is available free of charge at https://pubs.acs.org/doi/10.1021/acs.jpclett.2c02509.

Sample preparation procedure, description and results of characterization of the samples with powder X-ray diffraction, profilometry, and thermogravimetric analysis, description of linear and two-dimensional infrared spectroscopic experiments, additional FTIR spectra 2D-IR spectra and pump-integrated slices, and analysis of the $\nu_{as} \rightarrow \nu_{Ph}$ and $\nu_{Ph} \rightarrow \nu_{as}$ cross-peak signal dynamics, analysis of the temperature dependence of the FTIR spectra of the UiO-66 membranes and interpretation of signals at long waiting times (PDF)

Transparent Peer Review report available (PDF)

■ AUTHOR INFORMATION

Corresponding Author

Alexander A. Korotkevich − *AMOLF, Ultrafast Spectroscopy, 1098 XG Amsterdam, The Netherlands;* orcid.org/0000-0002-0775-752X; Email: a.korotkevich@amolf.nl

Authors

Oleksandr O. Sofronov − *AMOLF, Ultrafast Spectroscopy, 1098 XG Amsterdam, The Netherlands;* orcid.org/0000-0001-7744-6404

Olivier Lugier − *Functional Materials Group, Van't Hoff Institute for Molecular Sciences (HIMS), Universiteit van Amsterdam, 1098 XH Amsterdam, The Netherlands*

Sanghamitra Sengupta − *AMOLF, Ultrafast Spectroscopy, 1098 XG Amsterdam, The Netherlands;* orcid.org/0000-0002-3984-1857

Stefania Tanase − *Functional Materials Group, Van't Hoff Institute for Molecular Sciences (HIMS), Universiteit van Amsterdam, 1098 XH Amsterdam, The Netherlands;* orcid.org/0000-0003-2830-1924

Huib J. Bakker − *AMOLF, Ultrafast Spectroscopy, 1098 XG Amsterdam, The Netherlands;* orcid.org/0000-0003-1564-5314

Complete contact information is available at: https://pubs.acs.org/10.1021/acs.jpclett.2c02509

Author Contributions

§A.A.K. and O.O.S. contributed equally to this work.

Notes

The authors declare no competing financial interest.

■ ACKNOWLEDGMENTS

This work is part of the research program of The Netherlands Organization for Scientific Research (NWO) and was performed at the research institute AMOLF. This project has received funding from the European Research Council (ERC) under the European Unions Horizon 2020 research and innovation program (Grant Agreement 694386). The authors thank Niels Winkelaar for cutting the sapphire wafers, Ricardo Struik and Hinco Schoenmaker for making the sample holder for running the reactions, Bob Drent for assistance with profilometry measurements, Dr. Jan Versluis for assistance with the 2D-IR setup, and Dr. Sonia Castellanos Ortega for meaningful suggestions and fruitful discussions.

■ REFERENCES

(1) Eddaoudi, M.; Kim, J.; Rosi, N.; Vodak, D.; Wachter, J.; O'Keeffe, M.; Yaghi, O. M. Systematic Design of Pore Size and Functionality in Isoreticular MOFs and Their Application in Methane Storage. *Science* **2002**, *295*, 469−472.

(2) Burrows, A. D. Mixed-Component Metal-Organic Frameworks (MC-MOFs): Enhancing Functionality through Solid Solution Formation and Surface Modifications. *CrystEngComm* **2011**, *13*, 3623−3642.

(3) Xue, D.-X.; Belmabkhout, Y.; Shekhah, O.; Jiang, H.; Adil, K.; Cairns, A. J.; Eddaoudi, M. Tunable Rare Earth fcu-MOF Platform: Access to Adsorption Kinetics Driven Gas/Vapor Separations via Pore Size Contraction. *J. Am. Chem. Soc.* **2015**, *137*, 5034−5040.

(4) Razavi, S. A. A.; Masoomi, M. Y.; Islamoglu, T.; Morsali, A.; Xu, Y.; Hupp, J. T.; Farha, O. K.; Wang, J.; Junk, P. C. Improvement of Methane-Framework Interaction by Controlling Pore Size and Functionality of Pillared MOFs. *Inorg. Chem.* **2017**, *56*, 2581−2588.

(5) Wen, Y.; Zhang, J.; Xu, Q.; Wu, X.-T.; Zhu, Q.-L. Pore Surface Engineering of Metal-Organic Frameworks for Heterogeneous Catalysis. *Coord. Chem. Rev.* **2018**, *376*, 248−276.

(6) Wang, X.-F.; Song, X.-Z.; Sun, K.-M.; Cheng, L.; Ma, W. MOFs-Derived Porous Nanomaterials for Gas Sensing. *Polyhedron* **2018**, *152*, 155−163.

(7) Li, B.; Wen, H.-M.; Zhou, W.; Chen, B. Porous Metal-Organic Frameworks for Gas Storage and Separation: What, How, and Why? *J. Phys. Chem. Lett.* **2014**, *5*, 3468−3479.
(8) He, B.; Dong, X. Hierarchically Porous Zr-MOFs Labelled Methylene Blue as Signal Tags for Electrochemical Patulin Aptasensor Based on ZnO Nano Flower. *Sens. Actuators B Chem.* **2019**, *294*, 192−198.
(9) Wang, H.-F.; Chen, L.; Pang, H.; Kaskel, S.; Xu, Q. MOF-Derived Electrocatalysts for Oxygen Reduction, Oxygen Evolution and Hydrogen Evolution Reactions. *Chem. Soc. Rev.* **2020**, *49*, 1414−1448.
(10) Cavka, J. H.; Jakobsen, S.; Olsbye, U.; Guillou, N.; Lamberti, C.; Bordiga, S.; Lillerud, K. P. A New Zirconium Inorganic Building Brick Forming Metal Organic Frameworks with Exceptional Stability. *J. Am. Chem. Soc.* **2008**, *130*, 13850−13851.
(11) Valenzano, L.; Civalleri, B.; Chavan, S.; Bordiga, S.; Nilsen, M. H.; Jakobsen, S.; Lillerud, K. P.; Lamberti, C. Disclosing the Complex Structure of UiO-66 Metal- Organic Framework: a Synergic Combination of Experiment and Theory. *Chem. Mater.* **2011**, *23*, 1700−1718.
(12) Winarta, J.; Shan, B.; Mcintyre, S. M.; Ye, L.; Wang, C.; Liu, J.; Mu, B. A Decade of UiO-66 Research: A Historic Review of Dynamic Structure, Synthesis Mechanisms, and Characterization Techniques of an Archetypal Metal-Organic Framework. *Cryst. Growth Des.* **2020**, *20*, 1347−1362.
(13) Khudozhitkov, A. E.; Arzumanov, S. S.; Kolokolov, D. I.; Stepanov, A. G. UiO-66 (Zr) MOF as a Promising Material for Butane Isomers Separation: Evidence Based on the Analysis of the Adsorbed Alkanes Mobility by 2H NMR and Molecular Dynamics Simulation. *J. Phys. Chem. C* **2021**, *125*, 13391−13400.
(14) Virmani, E.; Rotter, J. M.; Mähringer, A.; von Zons, T.; Godt, A.; Bein, T.; Wuttke, S.; Medina, D. D. On-Surface Synthesis of Highly Oriented Thin Metal-Organic Framework Films through Vapor-Assisted Conversion. *J. Am. Chem. Soc.* **2018**, *140*, 4812−4819.
(15) Miyamoto, M.; Hori, K.; Goshima, T.; Takaya, N.; Oumi, Y.; Uemiya, S. An Organoselective Zirconium-Based Metal-Organic-Framework UiO-66 Membrane for Pervaporation. *Eur. J. Inorg. Chem.* **2017**, *2017*, 2094−2099.
(16) Liu, X. Metal-organic framework UiO-66 membranes. *Front. Chem. Sci. Eng.* **2020**, *14*, 216−232.
(17) Cmarik, G. E.; Kim, M.; Cohen, S. M.; Walton, K. S. Tuning the Adsorption Properties of UiO-66 via Ligand Functionalization. *Langmuir* **2012**, *28*, 15606−15613.
(18) Johnson, B. A.; Bhunia, A.; Fei, H.; Cohen, S. M.; Ott, S. Development of a UiO-Type Thin Film Electrocatalysis Platform with Redox-Active Linkers. *J. Am. Chem. Soc.* **2018**, *140*, 2985−2994.
(19) Sun, Y.; Song, C.; Guo, X.; Liu, Y. Concurrent Manipulation of Out-of-Plane and Regional In-Plane Orientations of NH2-UiO-66 Membranes with Significantly Reduced Anisotropic Grain Boundary and Superior H2/CO2 Separation Performance. *ACS Appl. Mater. Interfaces* **2020**, *12*, 4494−4500.
(20) Yang, F.; Huang, H.; Wang, X.; Li, F.; Gong, Y.; Zhong, C.; Li, J.-R. Proton Conductivities in Functionalized UiO-66: Tuned Properties, Thermogravimetry Mass, and Molecular Simulation Analyses. *Cryst. Growth Des.* **2015**, *15*, 5827−5833.
(21) Wang, X.; Zhai, L.; Wang, Y.; Li, R.; Gu, X.; Yuan, Y. D.; Qian, Y.; Hu, Z.; Zhao, D. Improving Water-Treatment Performance of Zirconium Metal-Organic Framework Membranes by Postsynthetic Defect Healing. *ACS Appl. Mater. Interfaces* **2017**, *9*, 37848−37855.
(22) Xiang, W.; Ren, J.; Chen, S.; Shen, C.; Chen, Y.; Zhang, M.; Liu, C.-j. The Metal-Organic Framework UiO-66 with Missing-Linker Defects: a Highly Active Catalyst for Carbon Dioxide Cycloaddition. *Appl. Energy* **2020**, *277*, 115560.
(23) Feng, L.; Hou, H.-B.; Zhou, H. UiO-66 Derivatives and Their Composite Membranes for Effective Proton Conduction. *Dalton Trans.* **2020**, *49*, 17130−17139.
(24) Wu, H.; Chua, Y. S.; Krungleviciute, V.; Tyagi, M.; Chen, P.; Yildirim, T.; Zhou, W. Unusual and Highly Tunable Missing-Linker Defects in Zirconium Metal-Organic Framework UiO-66 and Their Important Effects on Gas Adsorption. *J. Am. Chem. Soc.* **2013**, *135*, 10525−10532.
(25) Clark, C. A.; Heck, K. N.; Powell, C. D.; Wong, M. S. Highly Defective UiO-66 Materials for the Adsorptive Removal of Perfluorooctanesulfonate. *ACS Sustain. Chem. Eng.* **2019**, *7*, 6619−6628.
(26) Feng, X.; Jena, H. S.; Krishnaraj, C.; Leus, K.; Wang, G.; Chen, H.; Jia, C.; van der Voort, P. Generating Catalytic Sites in UiO-66 through Defect Engineering. *ACS Appl. Mater. Interfaces* **2021**, *13*, 60715−60735.
(27) Cirujano, F. G.; Llabrés i Xamena, F. X. Tuning the Catalytic Properties of UiO-66 Metal-Organic Frameworks: From Lewis to Defect-Induced Brønsted Acidity. *J. Phys. Chem. Lett.* **2020**, *11*, 4879−4890.
(28) Borges, D. D.; Devautour-Vinot, S.; Jobic, H.; Ollivier, J.; Nouar, F.; Semino, R.; Devic, T.; Serre, C.; Paesani, F.; Maurin, G. Proton Transport in a Highly Conductive Porous Zirconium-Based Metal-Organic Framework: Molecular Insight. *Angew. Chem., Int. Ed.* **2016**, *55*, 3919−3924.
(29) Ling, S.; Slater, B. Dynamic Acidity in Defective UiO-66. *Chem. Sci.* **2016**, *7*, 4706−4712.
(30) Balčiūnas, S.; Pavlovaitė, D.; Kinka, M.; Yeh, J.-Y.; Han, P.-C.; Shieh, F.-K.; Wu, K. C.-W.; Šimėnas, M.; Grigalaitis, R.; Banys, J. Dielectric Spectroscopy of Water Dynamics in Functionalized UiO-66 Metal-Organic Frameworks. *Molecules* **2020**, *25*, 1962.
(31) Gutierrez, M.; Cohen, B.; Sánchez, F.; Douhal, A. Photochemistry of Zr-based MOFs: Ligand-to-Cluster Charge Transfer, Energy Transfer and Excimer Formation, What Else Is There? *Phys. Chem. Chem. Phys.* **2016**, *18*, 27761−27774.
(32) Liu, J.; Jiang, S.-l.; Zhang, Q. Doping Copper Ions in a Metal-Organic Framework (UiO-66-NH2): Location Effect Examined by Ultrafast Spectroscopy. *Chin. J. Chem. Phys.* **2020**, *33*, 394−400.
(33) Nishida, J.; Tamimi; Fei, H.; Pullen, S. P.; Ott, S.; Cohen, S. M.; Fayer, M. D. Structural Dynamics Inside a Functionalized Metal-Organic Framework Probed by Ultrafast 2D IR Spectroscopy. *Proc. Natl. Acad. Sci. U.S.A* **2014**, *111*, 18442−18447.
(34) Nishida, J.; Fayer, M. D. Guest Hydrogen Bond Dynamics and Interactions in the Metal-Organic Framework MIL-53(Al) Measured with Ultrafast Infrared Spectroscopy. *J. Phys. Chem. C* **2017**, *121*, 11880−11890.
(35) Yan, J.; Sun, Y.; Ji, T.; Zhang, C.; Liu, L.; Liu, Y. Room-Temperature Synthesis of Defect-Engineered Zirconium-MOF Membrane Enabling Superior CO2/N2 Selectivity with Zirconium-Oxo Cluster Source. *J. Membr. Sci.* **2022**, *653*, 120496.
(36) Wang, X.; Lyu, Q.; Tong, T.; Sun, K.; Lin, L.-C.; Tang, C. Y.; Yang, F.; Guiver, M. D.; Quan, X.; Dong, Y. Robust Ultrathin Nanoporous MOF Membrane with Intra-Crystalline Defects for Fast Water Transport. *Nat. Commun.* **2022**, *13*, 266.
(37) Wilson, E. B. The Normal Modes and Frequencies of Vibration of the Regular Plane Hexagon Model of the Benzene Molecule. *Phys. Rev.* **1934**, *45*, 706−714.
(38) Arenas, J.; Marcos, J. Infrared and Raman spectra of Phtalate, Isophtalate and Terephtalate Ions. *Spectrochim. Acta A Mol.* **1979**, *35*, 355−363.
(39) Boerio, F. J.; Roth, P. G. Vibrational Analysis of Terephthalate and Terephthalate-D4 Ions. *Appl. Spectrosc.* **1987**, *41*, 463−467.
(40) Varghese, H. T.; Panicker, C. Y.; Philip, D.; Sreevalsan, K.; Anithakumary, V. IR, Raman and SERS Spectra of Disodium Terephthalate. *Spectrochim. Acta A Mol. Biomol* **2007**, *68*, 817−822.
(41) Korotkevich, A. A.; Bakker, H. J. Ultrafast Vibrational Dynamics of Aqueous Acetate and Terephthalate. *J. Chem. Phys.* **2022**, *156*, 094501.
(42) Hamm, P.; Zanni, M.*Concepts and methods of 2D infrared spectroscopy*; Cambridge University Press: Cambridge, U.K., 2011; pp 109−144.
(43) Rezus, Y. L. A.; Bakker, H. J. Orientational Dynamics of Isotopically Diluted H_2O and D_2O. *J. Chem. Phys.* **2006**, *125*, 144512.
(44) Lotze, S.; Groot, C. C. M.; Vennehaug, C.; Bakker, H. J. Femtosecond Mid-Infrared Study of the Dynamics of Water

https://doi.org/10.1021/acs.jpclett.2c02509
J. Phys. Chem. Lett. 2022, 13, 9793−9800

Molecules in Water-Acetone and Water-Dimethyl Sulfoxide Mixtures. *J. Phys. Chem. B* **2015**, *119*, 5228−5239.
(45) Korotkevich, A. A.; Bakker, H. J. Confined Water Molecules in Binary Mixtures of Water and 2,6-Lutidine Near Lower Solution Critical Temperature. *J. Phys. Chem. B* **2021**, *125*, 287−296.
(46) Andreeva, A. B.; Le, K. N.; Chen, L.; Kellman, M. E.; Hendon, C. H.; Brozek, C. K. Soft Mode Metal-Linker Dynamics in Carboxylate MOFs Evidenced by Variable-Temperature Infrared Spectroscopy. *J. Am. Chem. Soc.* **2020**, *142*, 19291−19299.

https://doi.org/10.1021/acs.jpclett.2c02509
J. Phys. Chem. Lett. 2022, 13, 9793−9800